STRUCTURAL SCIENCE
CRYSTAL ENGINEERING
MATERIALS

Volume 79 (2023)

Supporting information for article:

A rod- and tessellation-based comparative analysis of polymorphic and structurally-invariant molecular crystals: application to sulfathiazole and 2-benzyl-5-benzylidenecyclopentanones

Noel W. Thomas and David S. Hughes

Supporting information for the article entitled

A rod- and tessellation-based comparative analysis of polymorphic and structurally invariant molecular crystals: application to sulfathiazole and 2-benzyl-5-benzylidenecyclopentanones

Authors

Noel W. Thomas[a]* and David S. Hughes[b]

[a]Werkstofftechnik Glas & Keramik, Hochschule Koblenz, Rheinstrasse 56, 56203 Hoehr-Grenzhausen, Germany

[b]Yusuf Hamied Department of Chemistry, University of Cambridge, Lensfield Road, Cambridge, CB2 1EW, United Kingdom

Correspondence email: thomas@hs-koblenz.de

S1. The resetting of $P2_1/n$ structures in the standard setting, $P2_1/c$

Equations (S1) define the transformation equations for the unit cell vectors, whereby the unprimed vectors refer to space group $P2_1/n$ and the primed vectors to $P2_1/c$.

$$\begin{aligned} \boldsymbol{a}' &= \mathbf{c} \\ \boldsymbol{b}' &= \boldsymbol{b} \\ \boldsymbol{c}' &= -[\boldsymbol{c} + \boldsymbol{a}] \end{aligned} \qquad \text{(S1)}$$

The required transformation matrix $\boldsymbol{P}$ is given by equation (S2), whereby the notation of Hahn (1995) has been adopted.

$$(\boldsymbol{a}' \quad \boldsymbol{b}' \quad \boldsymbol{c}') = (\boldsymbol{a} \quad \boldsymbol{b} \quad \boldsymbol{c})\boldsymbol{P} \quad \text{with} \quad \boldsymbol{P} = \begin{pmatrix} 0 & 0 & -1 \\ 0 & 1 & 0 \\ 1 & 0 & -1 \end{pmatrix} \qquad \text{(S2)}$$

Accordingly, the matrix to transform coordinates from the $P2_1/n$ to the $P2_1/c$ setting is given by equation (S3).

$$\boldsymbol{Q} = \boldsymbol{P}^{-1} = \begin{pmatrix} -1 & 0 & 1 \\ 0 & 1 & 0 \\ -1 & 0 & 0 \end{pmatrix} \qquad \text{(S3)}$$

The relationship of the crystal axes in $P2_1/c$ to those in $P2_1/n$ is highlighted in Fig. S1 for Polymorph V of sulfathiazole.

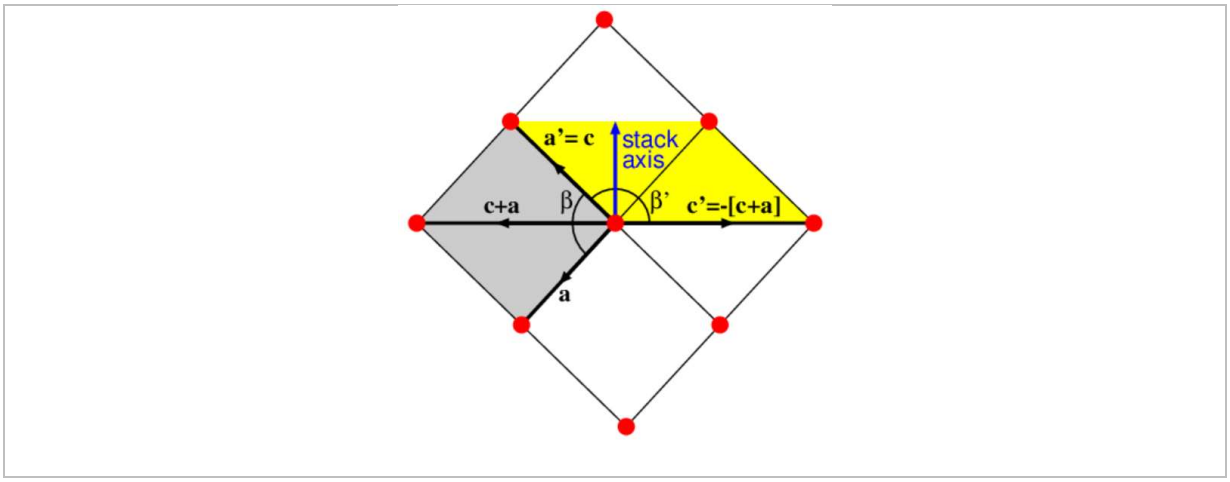

Figure S1 Inter-relationship of space groups $P2_1/n$ and $P2_1/c$. Red circles: lattice points; grey parallelogram: $P2_1/n$ unit cell; yellow parallelogram: $P2_1/c$ unit cell. The stack axis, which is normal to the *b'c'*-plane, joins bottom and top of the $P2_1/c$ unit cell. The *b*- and *b'*-axes are directed perpendicular to the diagram.

The original and transformed unit cell axes for polymorphs V (Hughes, 2003) and II (Hughes *et al.*, 1999) of sulfathiazole are quoted in Table S1.

Table S1 Listing of unit cell constants for polymorphs V and II of sulfathiazole

Polymorph	$P2_1/n$ setting	$P2_1/c$ setting
V	*a*=10.774 Å *b*=8.467 Å *c*=11.367 Å β= 91.65°	*a*=11.367 Å *b*=8.467 Å *c*= 15.435 Å β=135.75°
II	*a*=10.399 Å *b*=15.132 Å *c*= 14.280 Å β=91.21°	*a*=14.280 Å *b*=15.132 Å *c*= 17.487 Å β=143.52°

The stack axis shown in Fig. S1 is the reference axis adopted in the current work.

S2. Tessellation graphics for Polymorphs V and III

Tessellation graphics for Polymorph V in the sections of maximum φ_{2D} value at x=0.2828 and maximum symmetry at *x*=½ are shown in Fig. S2.

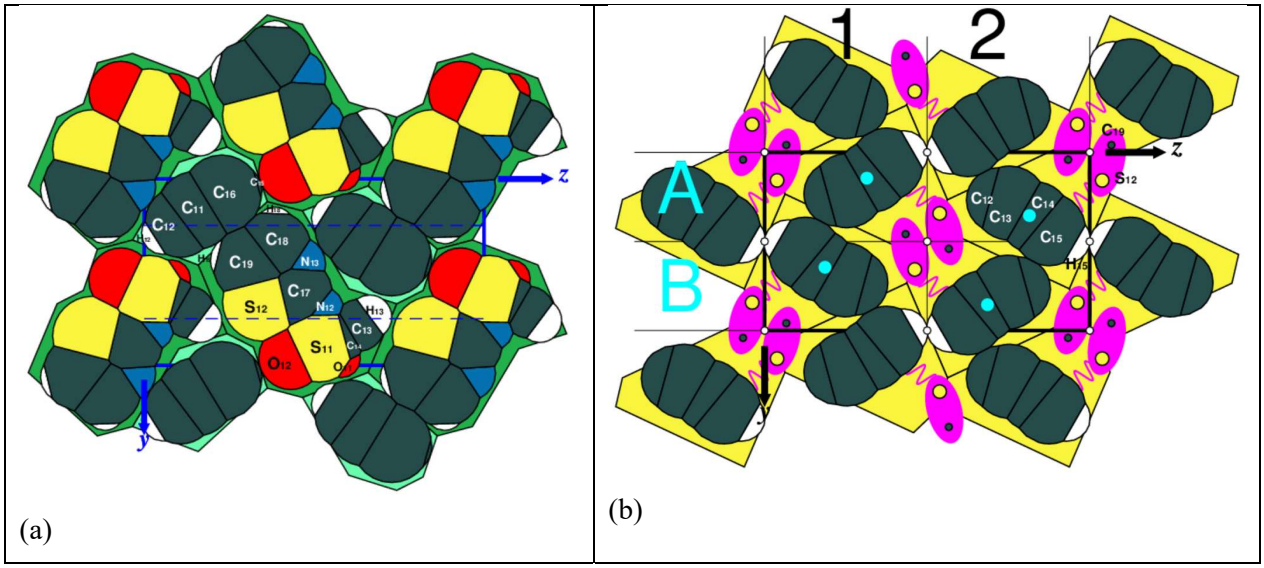

Figure S2 Tessellation diagrams for Polymorph V (a) at x=0.2828 and (b) at x=½.

The same set of atoms contributes to the section of maximum φ_{2D} as in the maximum φ_{2D} plane in Polymorph IV (Fig. 4(c) of article). φ_{2D} is marginally higher, at 0.8745 *cf.* 0.8705 for Polymorph IV An orientation of the diagram similar to Fig. 4(c) is obtained in the symmetry-equivalent plane at x = 0.7172. The Dirichlet domains formed by intersections of rods with the x = ½ plane are given in Fig. S2(c), with great similarity to the x = ½ plane of Polymorph IV (Fig. 5(b)).

The x=0 section of Polymorph V is shown in Fig. S3(a). Atoms with thicker magenta boundaries

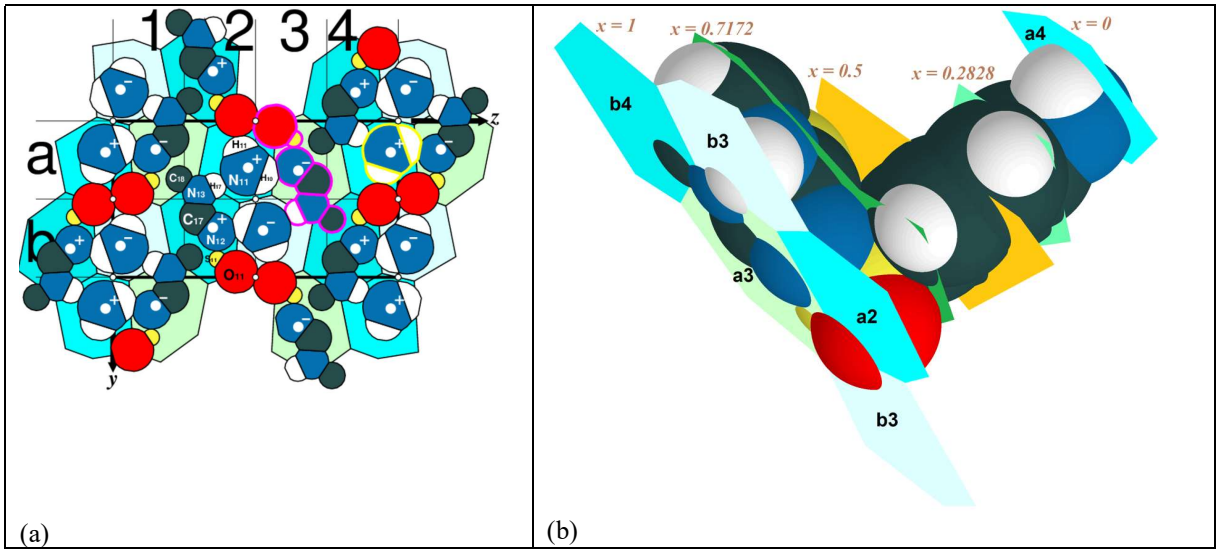

Figure S3 Polymorph V. (a) Dirichlet domains of residue centroids at x = 0. (b) corresponding minimum overlap view.

correspond to the atoms protruding from the plane labelled x=1 to the left of Fig. S3(b). Atoms with thicker yellow boundaries in Fig. S3(a) correlate with atoms permeating Dirichlet cell a4 at x=0, top right in Fig. S3(b). The orientation of Fig. S3(b) has been chosen to correlate to Fig. 6(b) in the article, which applies to Polymorph IV. It is inferred the general orientations of the molecules in

Polymorphs IV and V are similar. However, Polymorph V gives rise to a different JZ structure at x=0 and 1.

The two symmetry-independent sections of maximum φ_{2D} in Polymorph III are shown in Fig. S4.

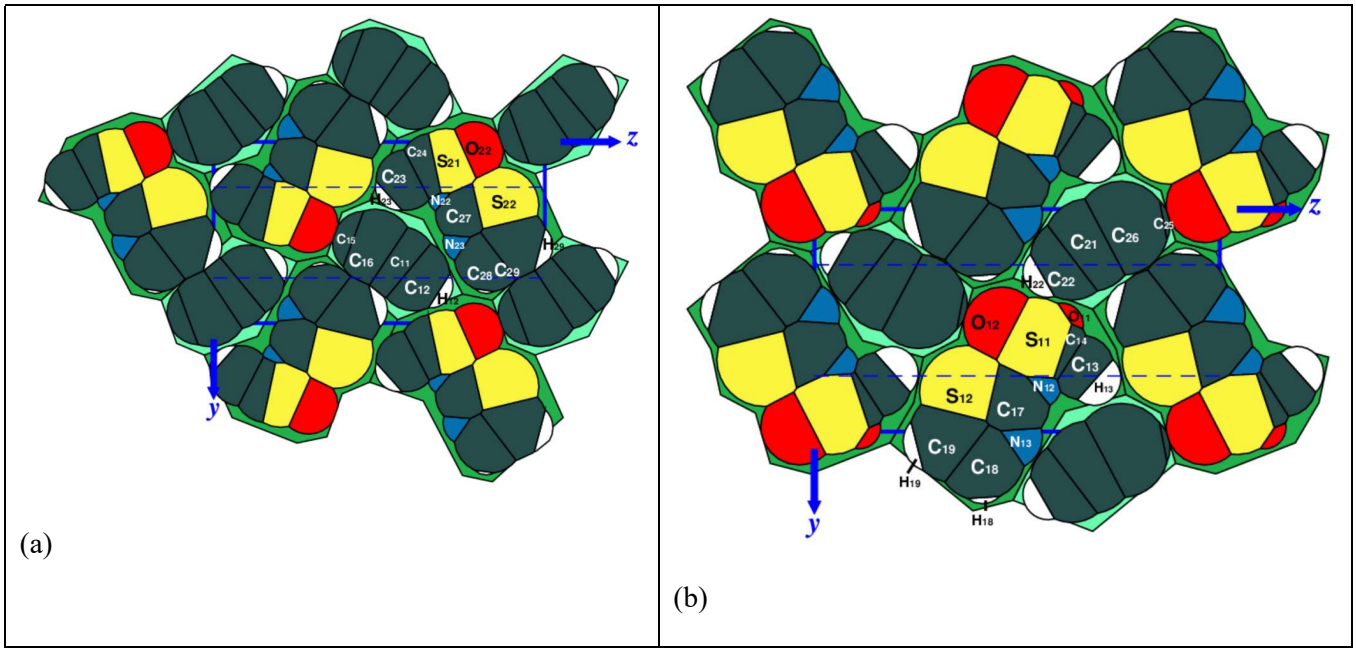

Figure S4 Planar sections of maximum φ_{2D} in sulfathiazole Polymorph III. (a) x=0.1531; (b) x=0.3529.

In Fig. S4(a), the thiazole molecular envelope of Molecule B is combined with the benzene molecular envelope of Molecule A, and in Fig. S4(b), the thiazole envelope of Molecule A is combined with the benzene envelope of Molecule B. The two symmetry-independent JZ at x=0 and x=½ are shown in Fig. S5.

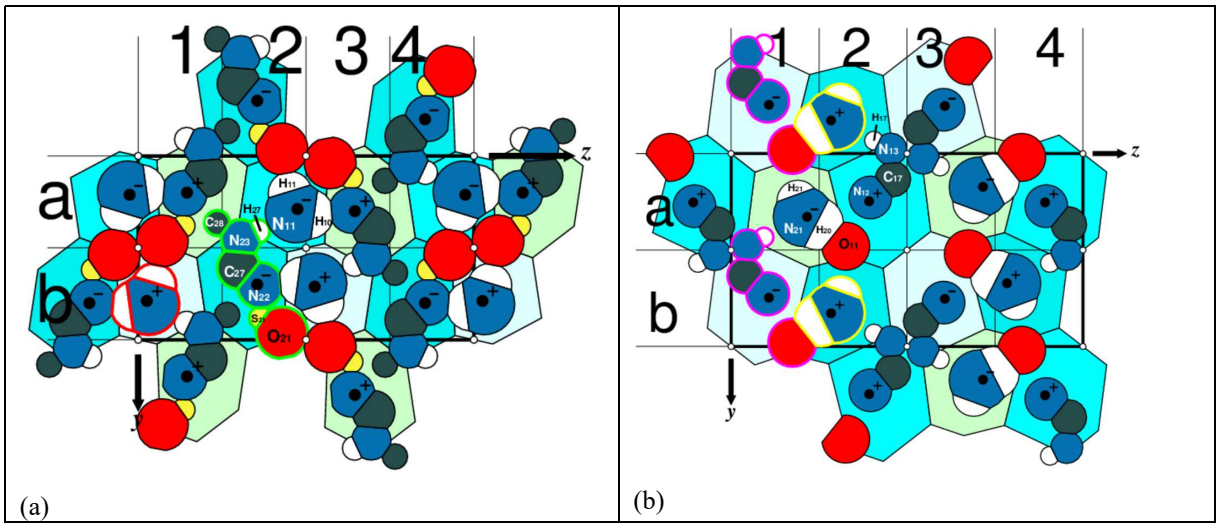

Figure S5 Tessellation diagrams for Polymorph III in maximum symmetry sections within JZ (a) at x=0; (b) at x=½.

Comparison of the φ_{2D} packing diagrams for Polymorphs IV, V and III in Figs. 3(a), 7(a) and 7(c) of the article leads to the expectation that the JZ at x=0 of Polymorph III be similar to the JZ of Polymorph V and that the JZ at x=½ of Polymorph III be similar to the JZ of Polymorph IV. This is seen to be the case, since Fig. S5(a) is similar to Fig. S3(a) and Fig. S5(b) to Fig. 5 of the article. This correlation is further observed in the two minimum overlap plots for Molecules A and B of Polymorph in Fig. S6. The protruding atoms to the left of Fig. S6(a) show a similar form to Fig. 6(d) of the article. Similarly the protruding atoms to the left of Fig. S6(a) have a similar form to Fig. S3(b).

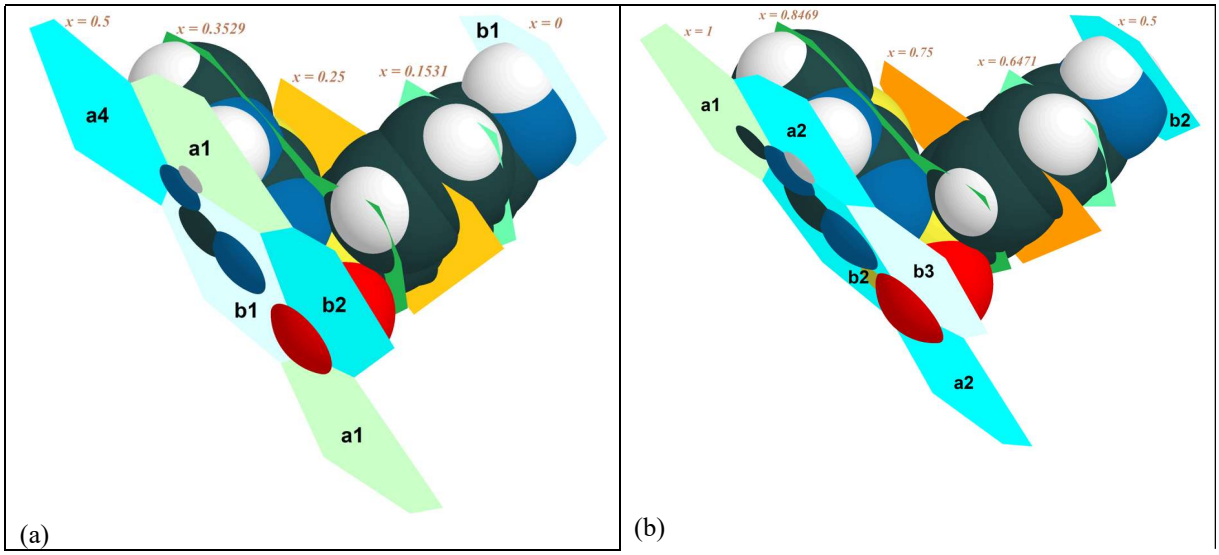

Figure S6 Polymorph III. Minimum overlap views of (a) Molecule A (with JZ formation at x=½) and (b) Molecule B (with JZ formation at x=1 or x=0), showing tessellation cells.

The transition from symmetry to pseudosymmetry between Polymorphs IV and V and III is observed at x=0.25 in Polymorph III (Fig. S7), where inversion symmetry no longer applies.

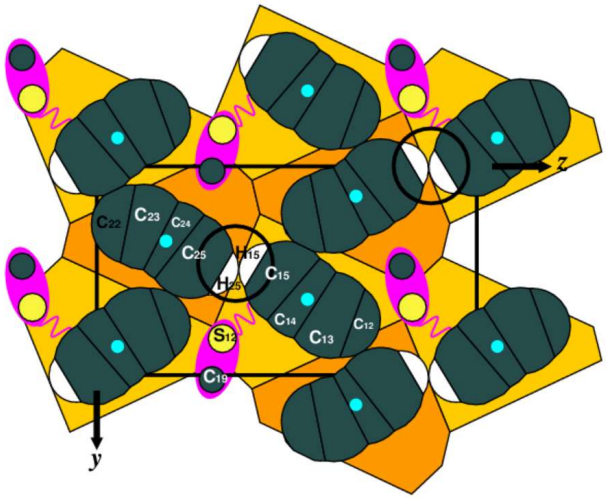

Figure S7 Polymorph III. Planar section at x = 0.25. Rod-based Dirichlet polygons of Molecules A are mustard-coloured and those for Molecule B coloured orange.

This may be directly seen through the loss of one set of C,S-satellite pairs compared to Fig. 5(b) of the article and Fig. S2(b). However, atoms H_{15} and H_{25} (encircled) are related by a pseudo-centre of inversion.

S3. Additional graphics relating to Polymorphs I and II of sulfathiazole

Graphics to complement §3.2 of the article are contained in this section. In Fig. S8(a) the x=0 section of Polymorph I is shown. This is a cut through the middle of the dimers shown in Figs. 10(a),(b),(c). N_{22}-H_{27}...N_{22}'-H_{27}' centrosymmetrically related dimers are enclosed in magenta circles. The associated N...H hydrogen bonds are revealed by the paired blue and white virtual semicircles, which result from overlapping atom spheres. The molecular envelopes corresponding to dimers of Molecules A (N_{12}-H_{17}...N_{12}'-H_{17}') are less apparent but nonetheless enclosed in yellow circles. The circle-fractions corresponding to N_{12} and N_{12}' are shaded in magenta to set them apart. There is also evidence of N_{21}-H_{21}···O_{21} H-bonding between pairs of Molecules B (see also Table 5). In this connection, non-bonded O_{21} and H_{21} atoms are enclosed in black circles. The interaction length, at 2.351 Å, is 0.34 Å shorter than the sum of the intermolecular radii. The centroid-based Dirichlet domains corresponding to the envelopes of Molecules A and B have comparable areas: 27.13 A^2 (orange background) and 28.47 $Å^2$ (green background), respectively.

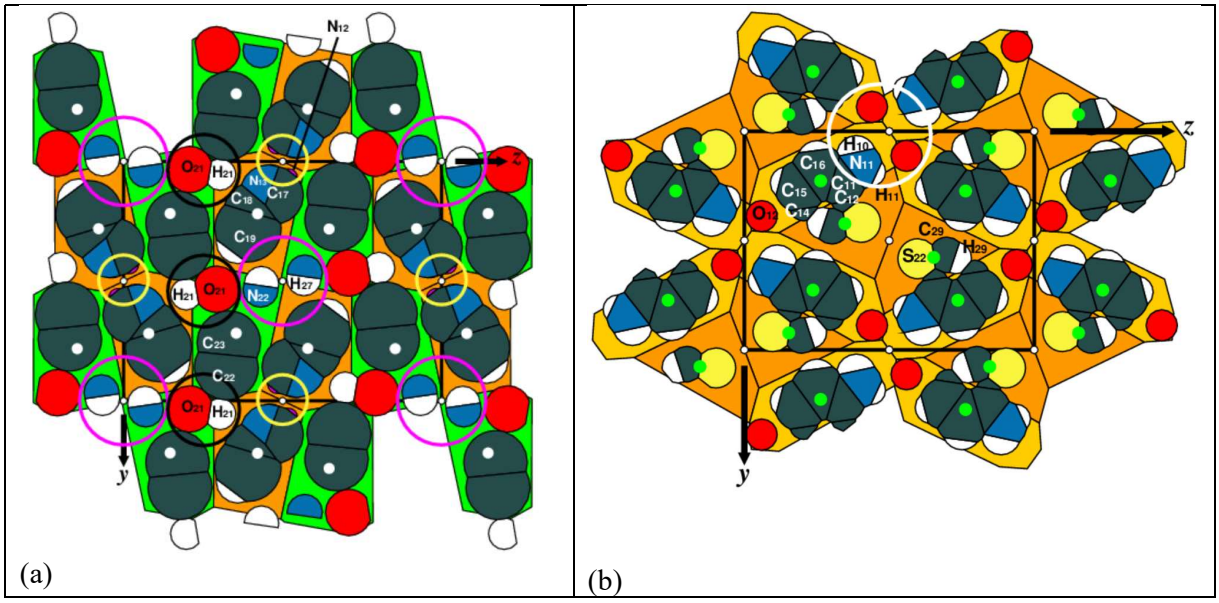

Figure S8 Polymorph I. (a) x=0 section; (b) x=½ section.

The x=½ section of Polymorph I in Fig. S4(b) is located at the centre of a broad minimum in φ_{2D} (Fig. 9(b)). The molecular envelopes are loosely packed, with the centroid-based Dirichlet domains of Molecules B, which result from S_{22}-C_{29}-H_{29} residues, only weakly reflecting envelope shape. Dirichlet domain areas are 32.17 $Å^2$ (mustard-coloured shading; Molecules A) and 23.42 $Å^2$ (orange shading; Molecules B). Oxygen atoms O_{12} and sulphur atoms S_{22} are disposed about the centres of symmetry. Molecules A form a 2D interconnected network of Dirichlet cells, which is associated with mutual

dispositions of oxygen atoms O_{12}, amine hydrogen atoms H_{11}, H_{12} and benzene ring atom H_{16} (encircled), which lead to attractive electrostatic interactions. A weak N_{11}-H_{11}···O_{12} hydrogen bond is listed in Table 5.

The 2D packing fraction is sufficiently high for MBCs to be constructed for the x=½ section of Polymorph II in Fig. S9(a). The outward-lying fractions of small circles for amine H_{11} atoms imply short non-bonded interactions. The shortest such interactions of these atoms are as follows: H_{11}...N_{12}': 2.132 Å; H_{11}...O_{11}': 2.535 Å; H_{11}...S_{11}': 2.925 Å. These are shorter than the sum of the intermolecular radii by respective amounts of 0.62, 0.16 and 0.05 Å, from which it is inferred that H...N interactions are predominantly stabilising. These correlate with a calculated potential energy of -6.22 kJ mol^{-1} in Table 5. The larger MBCs with orange background contain envelopes of Molecules A and the smaller MBCs with green background MBCs of Molecules B. Their areas are 46.796 and 19.357 Å^2 respectively, corresponding to a ratio of 2.418. This is significantly smaller than the Molecule B:Molecule A MBC ratio of 4.27 observed for the x=0 section (Fig. 10(e) of article). The section of Fig. S9(a) is a cut through the middle of the crowbar-shaped packing dimer, the atomic details of which are shown in minimum overlap view of Fig. S9(d).

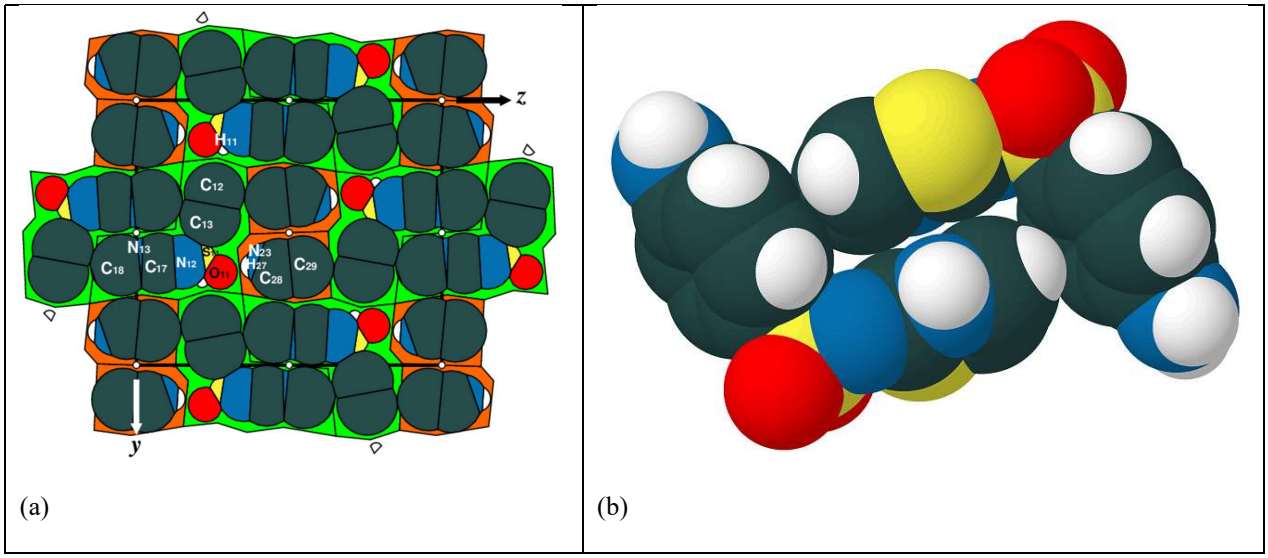

Figure S9 Polymorph II. (a) x=½ section; (b) structural details of the crowbar-shape formed by Molecules A in Fig. 10(d) of article.

S4. Substitutionally induced changes structure to types *c*, *d* and *e* in BBCP derivatives

An interesting facet of the BBCP derivatives is that, despite the three dominant structural types, three further completely different structural types, *c*, *d* and *e*, can be induced by appropriate substitutions. These are represented by the compounds *p*Cl-B *p*Br-BCP, B *o*Cl-BCP and B *m*Br-BCP, respectively, and are considered in the following three sub-sections.

S4.1. *p*Cl-B *p*Br-BCP

This compound can alternatively be regarded as the *p*Cl-benzyl derivative of B *p*Br-BCP, the *p*Br-benzylidene derivative of *p*Cl-BBCP or the compound *p*Me-B *p*Br-BCP with Cl substituted for Me. All three would be legitimate modelling starting-points. A sectional analysis of all three starting compounds $\perp yz$ indicates that stabilisation of *p*Cl-B *p*Br-BCP in structural type *a* (see Fig. 12(c)) would be sterically possible, as shown for *p*Me-B *p*Br-BCP at $x = 0.095$ in Fig. S10(a). This section lies within one of the special *x*-ranges highlighted in Fig. 13(a), in which six molecular residues co-exist. Thus the C_{20} atoms of the methyl groups, the bromo groups and the atoms of the benzene rings all belong to separate residues. It is seen that a structural accommodation of the adjacent methyl- and bromo-groups has taken place. However, the adoption by *p*Cl-B *p*Br-BCP of its own characteristic structural type, *c*, is indicative of an electronically induced repulsion of the chloro- and bromo-groups, which would be adjacent to each other in a type *a* structure. Structural type *c* is standard in the sense that it is based on centrosymmetrically related packing dimers and contains CPB and JZ. However, the inter-rod angle of 100.5° is untypically small and much closer to values found in sulfathiazole polymorphs (see Table 2). The change in packing dimer structure from photoreactive structure type *a* to photostable structure type *c* is shown in Figs. 12(c) and (d). The subtleness of the energy difference between structural types a and c has been experimentally verified by Theocharis *et al.* (1984) in forming mixed crystals of *p*Me-B *p*Br-BCP and *p*Cl-B *p*Br-BCP.

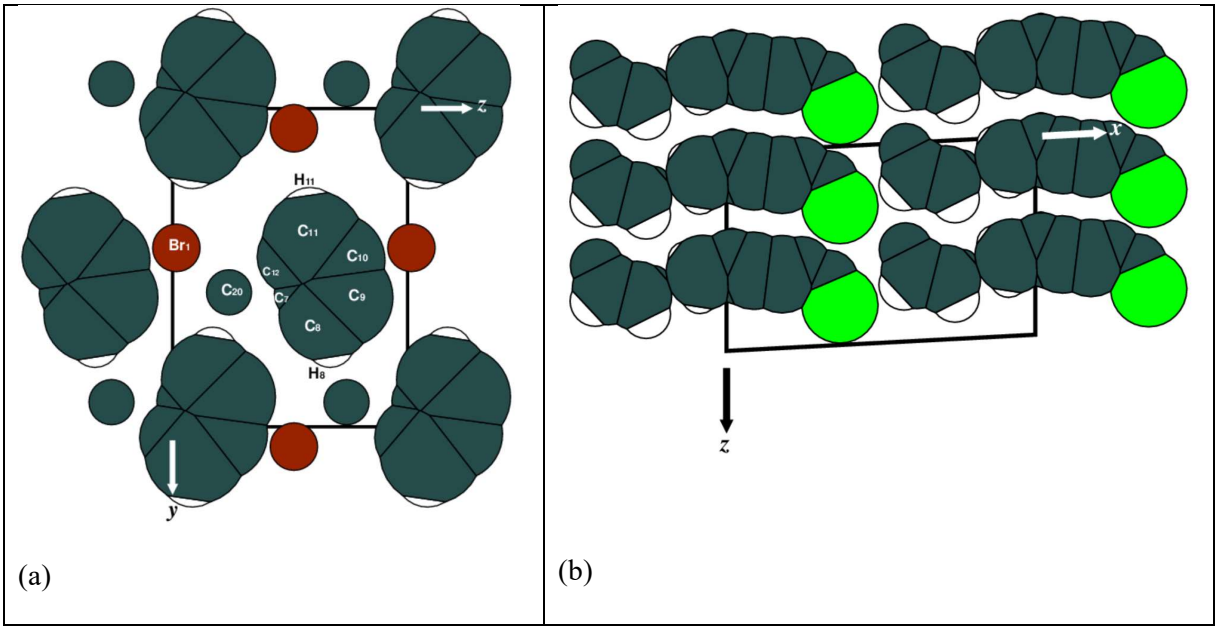

(a) (b)

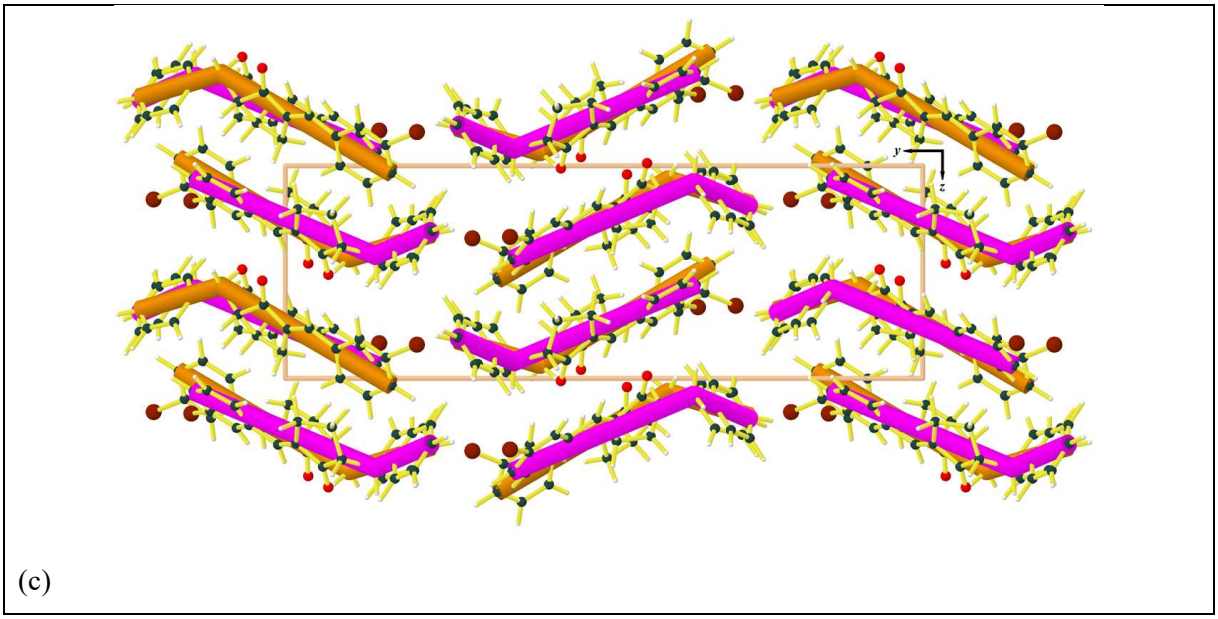

(c)

Figure S10 (a) x=0.95 section of *p*Me-B *p*Br-BCP showing the accommodation of both Me (C_{20} atom) and Br groups in a common section; (b) y=¼ section of B *o*Cl-BCP; (c) View of the B *m*Br-BCP structure $\perp yz$ (brown rods: Molecules A; magenta rods: Molecules B).

S4.2. B *o*Cl-BCP

It is surprising that this compound has its own structural type, since its related compound with a *larger* substituent, B *o*Br-BCP is stabilised within structural type *b*. The formation of this niche structure is related to the ability of space group $P2_1/c$ to support translationally related molecules in *y*-section, as observed for substituted anthracenes and anthraquinones with MBC of "Type 2" (Thomas, 2015). Special planes at y=¼ and y=¾ may be inferred by substituting y=¼ into positions (2) of the article:

1: x,¼,z; **4**: $x, ¼, z + \frac{1}{2}$ (S1)

2: $\bar{x}, ¾, \bar{z} + \frac{1}{2}$; **3**: $\bar{x}, ¾, \bar{z}$ (S2)

Positions (S1) give rise to two molecules in section at y=¼ that are related by a z-translation of ½. Positions (S2) define the symmetrically equivalent plane at y=¾. The section at y=¼ with two translationally related molecules per unit cell is shown in Fig. S10(b). This packing principle also allows the monoclinic angle to be tailored to the molecular shape. The dangling Cl-groups result from the *o*-substitutional position in the benzylidene moiety (Fig. 12(a)).

S4.3. B *m*Br-BCP

Since this is the only Z'=2 compound, it necessarily adopts its own structural type, *e*. The structure is characterised by a blocked structure along the *y*-axis with junction-zones at y=¼ and y=¾. The two

symmetry-independent molecules form cluster-pairs indicated in Fig. S10(c) by brown and magenta rods, respectively.

The intermolecular potential energies of interaction calculated with the potential set of Filippini & Gavezzotti (1993) are as follows: U_{AA} = -100.88 kJ mol^{-1}, U_{AB} = U_{BA} = -252.60 kJ mol^{-1} and U_{BB} = -104.09 kJ mol^{-1}. These values lead to an η_{SM} coefficient equal to 0.71 or 71%.

S5. Diagrams of axes linking centroid of molecular envelopes in junction zones of BBCP structural types *a*, *a'*, *b* and sulfathiazole polymorphs III, IV and V

Fig. S11 shows the axes linking centroids of molecular envelopes within the high-symmetry layers of junction zones for the six relevant prototype structures. The numerical values of the centroid coordinates are contained in Table 6 of the article. These are the axes about which the molecules are rotated to give rise to the results in Fig. 15.

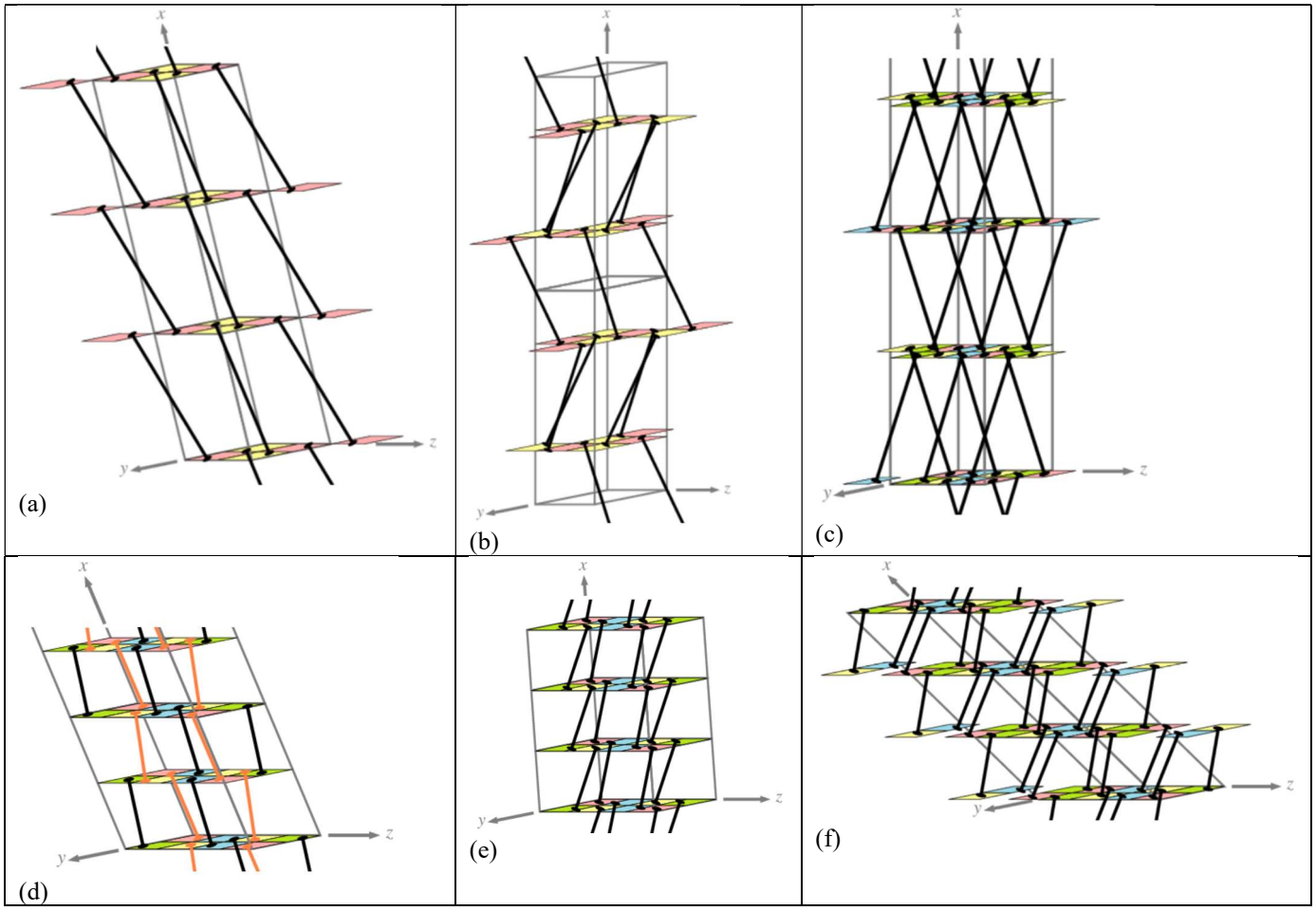

Figure S11 Axes of rotation joining JZ centroid coordinates in (a) *p*Cl-BBCP; (b) BBCP; (c) B *p*Cl-BCP; (d) sulfathiazole Polymorph III; (e) sulfathiazole Polymorph IV; (f) sulfathiazole Polymorph V.

S6. Comparison of hydrogen bond potential energies obtained for two alternative sets of non-bonded potentials

In this section, the results obtained from the Filippini & Gavezzotti (1993) (*FG*1993) and Gavezzotti (1994) (*GF*1994) sets of non-bonded potentials for hydrogen bond energies in Polymorphs III-V of sulfathiazole are compared. These underpin the systematic point that it is essential to use a potential set that is optimised for hydrogen bonding.

In defining a supramolecular cluster, as described in §2.5, the molecules identified as belonging to the cluster are strongly dependent on the potential parameters used. The *FG*1993 set was developed for organic molecular crystals without hydrogen bonds. By comparison, the *GF*1994 set is identical to *FG*1993 apart from special potentials for $\mathrm{X-H\cdots Y\ (X,Y=N,O)}$ hydrogen bonds.

Hughes (2003) identified, from a consideration of interaction-lengths, the potential hydrogen bonds listed in Tables S2 and S3 with nitrogen atoms as donors (X) and either oxygen or nitrogen atoms as acceptors (Y) on a neighbouring molecule. Whereas *FG*1993 predicts repulsive energies (with positive sign) for these hydrogen bonds, *GF*1994 correctly predicts attractive interactions (with negative sign). This difference is particularly marked for N_{13}-H_{17}···N_{11} interactions in Polymorph IV, with their potential energies changing from +22.06 to -27.25 kJ mol^{-1} (Table S2). *GF*1994 is therefore appropriate for modelling sulfathiazole structures.

Table S2 Calculated hydrogen bond energies of Polymorph IV for alternative sets of interatomic potentials: E_{FG}: *FG*1993; E_{GF}: *GF*1994.

Interaction of source molecule (1 0 0 0)	$d_{non\text{-}bonded}$ (Å)	Target molecule	E_{FG}(H..O) (kJ mol^{-1})	E_{FG}(H..N) (kJ mol^{-1})	E_{GF}(NH...O) (amides) (kJ mol^{-1})	E_{GF}(NH...N) (=N-H···N) (kJ mol^{-1})
N_{11}-H_{10}···O_{11}	2.131	(1 1 0 0)	+5.52		-9.67	
N_{11}-H_{11}···O_{11}	2.194	(2 0 0 0)	+3.61		-8.35	
N_{13}-H_{17}···N_{11}	1.973	(2 0 0 0)		+22.06		-27.25

The same conclusion emerges from a consideration of the hydrogen bond energies of Polymorphs V and III listed in Table S3. The most marked changes again relate to $N_{\$3}$-$H_{\$7}$···$N_{\$1}$ interactions, these changing as follows from positive to negative energies between *FG*1993 and *GF*1994:

Polymorph V: +16.00 to -24.00 kJ mol^{-1}; Polymorph III source molecule A: +21.80 to -27.13 kJ mol^{-1}; Polymorph III source molecule B: +18.62 kJ mol^{-1} to -25.52 kJ mol^{-1}.

Table S3 Calculated hydrogen bond energies of Polymorphs V and III for alternative sets of interatomic potentials. E_{FG}: *FG*1993; E_{GF}: *GF*1994.

Interaction	$d_{non\text{-}bonded}$ (Å)	Target molecule	E_{FG}(H..O) (kJ mol^{-1})	E_{FG}(H..N) (kJ mol^{-1})	E_{GF}(HB..O) (amides) (kJ mol^{-1})	E_{GF}(HB..N) (=N-H···N) (kJ mol^{-1})	E_{GF}(HB..N) (=NH_2···N) (kJ mol^{-1})
Polymorph V source molecule (1 0 0 0)							
N_{11}-H_{10}···N_{12}	2.366	(4 -1 0 -1)		+2.32			-5.53
N_{11}-H_{11}···O_{11}	2.176	(2 0 0 0)	+4.10		-8.71		
N_{13}-H_{17}···N_{11}	2.035	(2 0 0 0)		+16.00		-24.00	
Polymorph III source molecule A (1 0 0 0)							
N_{11}-H_{10}···N_{22}	2.354	B (3 -1 0 -1)		+2.52			-3.84
N_{11}-H_{11}···O_{21}	2.121	B (1 0 0 0)	+5.89		-9.90		
N_{13}-H_{17}···N_{21}	1.975	B (1 0 0 0)		+21.80		-27.13	
Polymorph III source molecule B (2 0 0 0)							
N_{21}-H_{20}···O_{11}	2.023	A (2 0 0 0)	+10.83		-12.33		
N_{21}-H_{21}···O_{11}	2.300	A (1 0 -1 0)	+1.56		-6.47		
N_{23}-H_{27}···N_{11}	2.006	A (1 0 -1 0)		+18.62		-25.52	

References

Filippini, G. & Gavezzotti, A. (1993). *Acta Cryst.* **B**49, 868–880.

Gavezzotti, A. & Filippini, G. (1994). *J. Phys. Chem.* **98**, 4831-4837.

Hughes, D.S. (2003). PhD thesis, University of Southampton.

Hughes, D. S., Hursthouse, M. B., Threlfall, T. L. and Tavener S. (1999). *Acta Cryst*. C**55**, 1831-1833.

Theocharis, C. R., Desiraju, G. R. & Jones, W. (1984). *J. Am. Chem. Soc*. **106**, 3606–3609

Thomas, N.W. (2015). *Acta Cryst.* B**71**, 463-477